# Automatic liver segmentation for volume measurement in CT Images

Seong-Jae Lim [a,*], Yong-Yeon Jeong [b], Yo-Sung Ho [a]

[a] *Gwangju Institute of Science and Technology (GIST), 1 Oryong-dong, Buk-gu, Gwangju 500-712, Republic of Korea*
[b] *Chonnam National University Medical School, 8 Hack-dong, Dong-gu, Gwangju 501-757, Republic of Korea*

## Abstract

Computed tomography (CT) images have been widely used for diagnosis of liver disease and volume measurement for liver surgery or transplantation. Automatic liver segmentation and volume measurement based on the segmentation are the most essential parts in computer-aided diagnosis for liver CT as well as computer-aided surgery. However, liver segmentation, in general, has been performed by outlining the medical image manually or segmenting CT images semi-automatically because surface features of the liver and partial-volume effects make automatic discrimination from other adjacent organs or tissues very difficult. Accordingly, in this paper, we propose a new approach to automatic segmentation of the liver for volume measurement in sequential CT images. Our method analyzes the intensity distribution of several abdominal CT samples and exploits a priori knowledge, such as CT numbers and location of the liver to identify coherent regions that correspond to the liver. The proposed scheme utilizes recursively morphological filter with region-labeling and clustering to detect the search range and to generate the initial liver contour. In this search range, we deform liver contour using the labeling-based search algorithm following pattern features of the liver contour. Lastly, volume measurement is automatically performed on the segmented liver regions. The experimental measurement of area and volume is compared with those using manual tracing method as a gold standard by the radiological doctors, and demonstrates that this algorithm is effective for automatic segmentation and volume measurement method of the liver.
© 2005 Elsevier Inc. All rights reserved.

*Keywords:* Liver segmentation; Volume measurement; Morphological filtering; Deformable contouring; Computer-aided diagnosis

## 1. Introduction

The liver cancer is one of the most common internal malignancies worldwide. The hepatocellular carcinoma is common in Asia and metastasis is common in the West. The liver cancer is also one of the leading death causes. Currently, the confirmed diagnosis used widely for the liver cancer is needle biopsy. The needle biopsy, however, is an invasive technique and generally not recommended [1]. Therefore, computed tomography (CT)

---

* Corresponding author. Fax: +82 62 970 2247.
  *E-mail addresses:* sjlim@gist.ac.kr (S.-J. Lim), yjeong@chonnam.ac.kr (Y.-Y. Jeong), hoyo@gist.ac.kr (Y.-S. Ho).

and magnetic resonance imaging (MRI) have been identified as accurate non-invasive imaging modalities in the diagnosis of the liver cancer. These medical images are interpreted by radiologists. However, image interpretation by human beings is often limited due to the non-systematic search patterns of themselves, the presence of structural noise in the image, and the presentation of complex disease states requiring the integration of vast amount of image data and clinical information.

Recently, computer-aided diagnosis (CAD), defined as a diagnosis introduced by a radiologist who uses the output from a computerized analysis of medical images as a ''second opinion'' in detecting lesions, assessing extent of disease, and making diagnostic decisions, is being used to improve the interpretation components of medical imaging [2,3]. In addition, computer-aided surgery (CAS) that is the future technology in surgery is performed on computerized surgical planning and image-guided surgery by analyzing region-of-interest (ROI) in the medical image. Volume measurement is also of major importance in different fields of medical imaging where physicians need some quantitative assessments for surgical decisions.

Research in CAD for both mammogram and chest radiographs is rapidly growing; however, CAD research for liver cancer is to be insufficient because the liver segmentation that plays an important role for CAD is difficult. This is mainly due to the two following facts. The first one is the proximity of the liver and other organs or muscles with the similar intensity. It makes difficult to resolve by observation of intensity discontinuity alone since partial-volume effects (PVE) cause the discontinuity to weaken where the structures touch. The second one is the variation in both shape and scale across patients even on the same patient [4].

There are many approaches for image segmentation, such as feature thresholding, contour based techniques, region based techniques, clustering, and template matching. Each of these approaches has its advantages and disadvantages in terms of applicability, suitability, performance, and computational cost [5]. Particularly, no one who did not consider above characteristics of the abdominal CT image can meet desirable results on liver segmentation. In addition, the traditional method of getting volume of the liver is to perform a by-hand 2D segmentation of parallel cross-sectional CT slices and to multiply all voxels of the stacked slices by their size while the procedure is often time consuming and non-systematic [6]. Therefore, to address above problems, we present an automatic liver segmentation algorithm in abdominal CT images using the combination of region-based and contour-based approaches. Our algorithm exploits both medical priori knowledge, for example, the general shape, location, and gray level of the liver, and deformable contour method using labeling-based search algorithm. Finally, total liver volumes were calculated from segmented areas of the liver to evaluate the patients for entire or partial liver transplantation and CAS.

This paper is organized as the following. In Section 2, we propose a new segmentation algorithm applicable to CT image, and we describe volume measurement in Section 3. After experimental results and analysis are presented in Section 4, we conclude the paper in Section 5.

## 2. Automatic liver segmentation

Mainly, the liver is approximated to muscle and gastrointestinal tract. Since adjacent organs have similar intensity with the liver as shown in Fig. 1, a direct liver-extraction approach without preprocessing may also extract undesirable boundaries resulting from its adjacent organs as fault positive/negative errors [1]. To cope with the problem, we present a new segmentation scheme with three stages. The first stage is image simplification as preprocessing; the second stage detects a search range detection with initial liver contour by using morphological filter; and the last stage is contour-based segmentation using labeling-based search algorithm that refines the initial liver boundary obtained in the second stage.

The overall framework of our proposed scheme is illustrated in Fig. 2. The input for algorithm is contrast enhanced, abdominal CT image of $512 \times 512$ pixels with gray level.

### 2.1. Image simplification

For image simplification, we consider a priori knowledge of the liver on abdominal CT image, such as shape, location, and intensity value. First of all, we decide ROI region. To identify ROI blocks, we divide the abdominal CT image into non-overlapping blocks of $64 \times 64$ pixels. Then, we discard the right-bottom region ('Rd' region except 'd1' block in Fig. 3) that is from a priori knowledge—the liver cannot be located
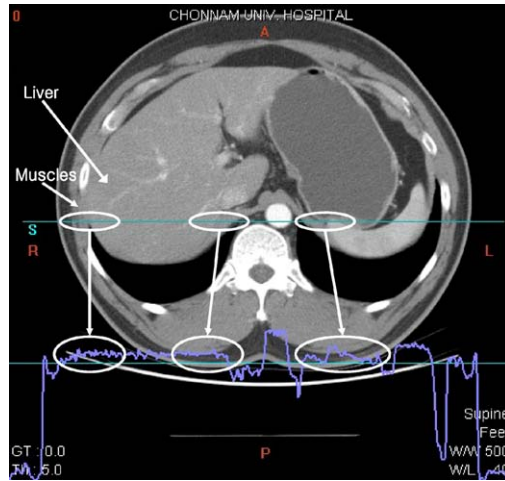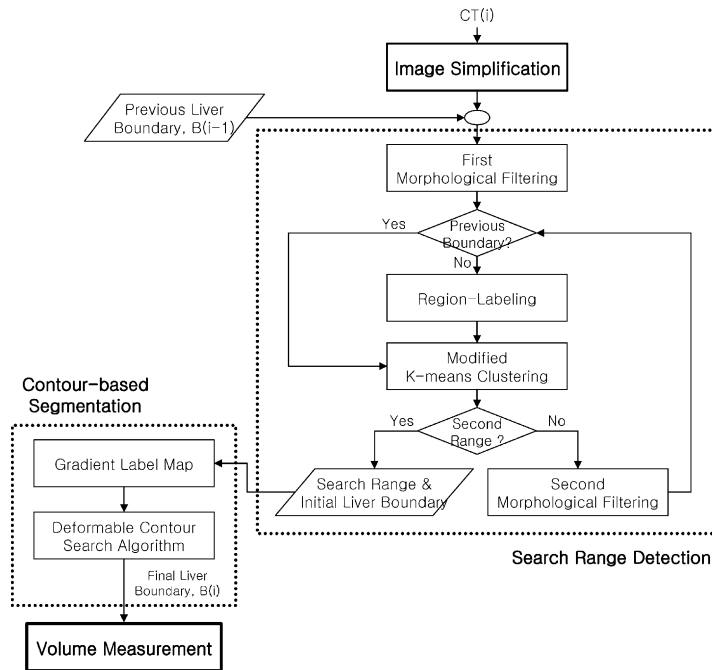
Fig. 1. Abdominal CT image.



Fig. 2. Block-diagram of the proposed algorithm.

in the right-bottom area but is generally located in the left side of CT images. Fig. 3 depicts ROI regions that are composed of 29 blocks of $64 \times 64$ pixels. Therefore, as shown in Fig. 3, the regions in this area cannot be part of the liver but can be eliminated so as to reduce the search area and computational efforts for liver boundary [2]. Second, we investigate and analyze the intensity distribution of several samples that are manually segmented liver and adjacent muscle. Fig. 4 illustrates the average intensity distribution of the liver and muscle. In addition, we interpret CT number (Hounsfield number) correspond to the liver and muscle into the gray level. Then, we decide threshold values for multilevel thresholding based on the statistical information by the above analysis in the ROI region. Multilevel thresholding based on the analysis of a priori knowledge makes many other organs or tissues disappear in ROI blocks and identifies the liver and adjacent region as clear or blur liver region. Fig. 5 shows the result of multilevel thresholding.
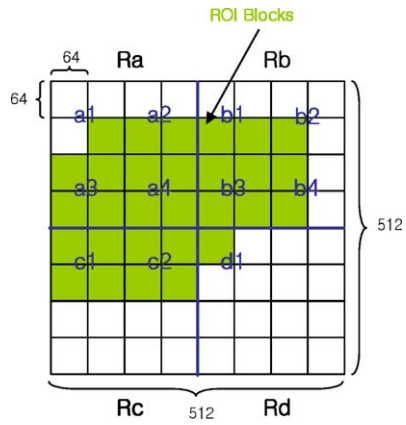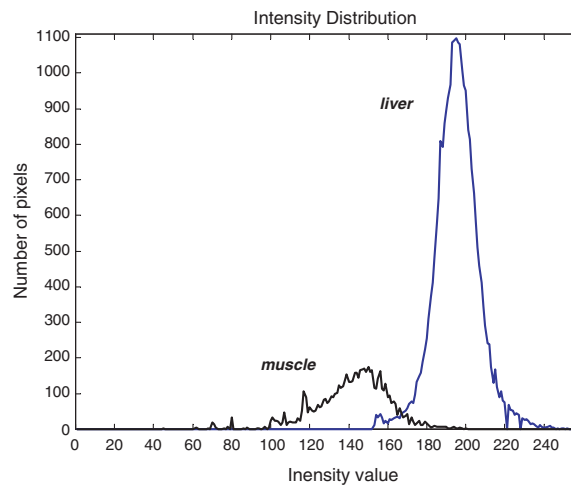
Fig. 3. ROI blocks.
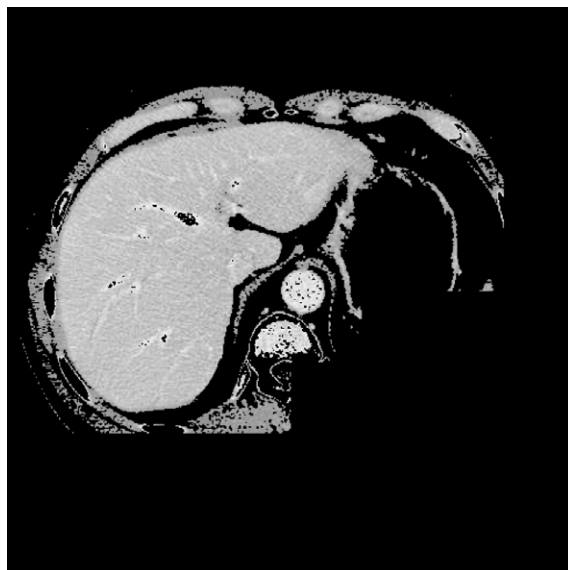


Fig. 4. Intensity distribution.



Fig. 5. Threshold image.

## 2.2. Search range detection

We present the search range to detect the precise liver boundary. For the search range, we find the first and second search region by performing multiscale morphological operations on the threshold image of the image simplification.

The following sections present the process of detecting search range for the liver boundary.

### 2.2.1. First multiscale morphological filtering

Image simplification classifies each pixel into clustered liver class and scattered non-liver class. Accordingly, we perform mathematical morphology filtering to reduce scattered class and detect liver object. This set theoretic, shape oriented approach treats the image as a set and the kernel of operation as another set, commonly known as structuring element (SE). Different standard morphological operations, namely (erosion, opening, closing, etc.) are basically set theoretic operations between these two sets. The shape and the size of the SE play important roles in detecting or extracting features of given shape and size from image [5].

In constructing a morphological filter, we use erosion and dilation with a flat SE as follows [7,8]:

$$(f \ominus B_n)(x,y) = \min\{f(x+l, y+m) | (l,m) \in B_n\}, \tag{1}$$

$$(f \oplus B_n)(x,y) = \max\{f(x-l, y-m) | (l,m) \in B_n\}. \tag{2}$$

Though the SE $B$ takes care of the shape of the features during processing the image, it cannot equally treat the objects of the same shape but of the different size. Thus, for processing objects based on their shape as well as size, we incorporate a second attribute to the SE, that is, its scale or composition. The types of morphological operations considered this are termed as multiscale morphology [9]. Multiscale filtering are defined, respectively, as

$$(f \ominus kB_n)(x,y) = \{(((f \ominus \underbrace{B_n) \ominus B_n) \cdots \ominus B_n}_{k \text{ times}})(x,y)\}, \tag{3}$$

$$(f \oplus kB_n)(x,y) = \{(((f \oplus \underbrace{B_n) \oplus B_n) \cdots \oplus B_n}_{k \text{ times}})(x,y)\}, \tag{4}$$

where $k$ is an integer representing the scale factor of the SE $B$ and $n$ is the size of $B$. Multiscale filtering is performed by using the composition of the $k$th order morphological erosion and dilation operations with the multisize SEs of the $5 \times 5$ and $3 \times 3$ flat size. The size of SEs is decided by analyzing the number of remained regions or pixels of the threshold image, and $k$ value is experimentally 4 or 5.

As previously mentioned, morphological filtering is operated on the ROI blocks in the threshold image. We recursively perform multiscale morphological filtering based on region-labeling and clustering to get the first search region and the second search region. The final search range is decided by excluding the second search region from the first search region. However, if the previous liver boundary is currently being used for segmenting the liver, region-labeling is omitted. The previous liver boundary approximately presents liver region in the current morphological filtered image because shape and location of the previous liver boundary is similar to the current liver boundary in consecutive CT images.

For the detection of the first search region, firstly, we find the initial liver region by performing multiscale morphological opening. In multiscale morphological opening, the erosion operation of $k$ times, as its first step eliminates bright features that do not fit within the SE and unconnected and scattered small features in the threshold image. Then, it dilates iteratively same times to the erosion operation to restore the contours of components that have not been completely removed by the first step. Fig. 6 shows the result of the multiscale morphological filtering.

### 2.2.2. Region-labeling

The performance of multiscale morphological filtering in the threshold image reduces the circumferential object of the liver, preserves the shape of the liver, and detects the initial liver region [2]. Yet, the larger composition order ('$k$' value) of the morphological filter, the looser regions of the liver. That is fixed order of morphological filtering composition removes the many parts of the liver of any patients. It is due to the various
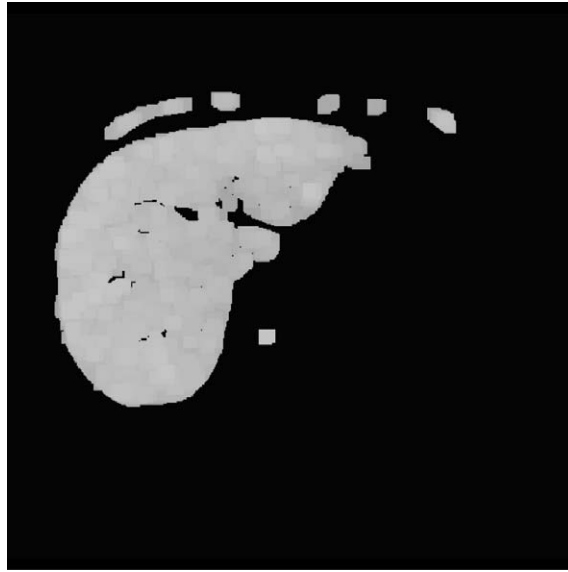
Fig. 6. Result of morphological filtering.

shape or size of the liver by patients. Thus, we use low order of morphological filtering to preserve the region of the liver. But, it can make more dispersed noises, such as the pixels of the other organs or muscles which have the similar intensity values with the liver. To reduce the noise of these kinds and detect the coarse liver region, we perform on the 4-connected region-labeling algorithm. The technique for region finding that is used in the region-labeling algorithm is breadth-first search approach [10]. After performing of the region-labeling algorithm, the largest labeled region is marked out for the candidate region of the liver.

### 2.2.3. Partition clustering

The result of region-labeling is the coarse liver region. This is due to the fact that adjoining non-liver organs and muscles are still remained. In order for detecting of the finer liver region, we classify the labeled image into three classes based on the result of morphological filtering. Region classifying is performed by the modified K-means algorithm. The adjoining tissues or muscles in the liver have mainly higher or lower intensity value than that of the liver. Therefore, we use three centroid for the modified K-means algorithm. However, the middle centroid corresponding to the mean value of the liver among three centroid is just computed again and the others are fixed to the max and min intensity value in labeled liver region. This processing divides the region into the adjacent noise of the liver and the liver region. After we reduce the class of the adjacent noise, we get the fine initial liver region. Finally, the image of the first search region is constructed by performing the different order's composition between erosion and dilation operation of the mathematical morphological opening on the clustered initial liver region as follows

$$(f \circ iB_n)(x,y) = ((f \ominus iB_n) \oplus (i+j)B_n)(x,y), \tag{5}$$

where $i$ is the scale factor of the SE $B$ and $j$ is a parameter which decides the size of search range. Generally, $i$ is 2 and $j$ is 4 or 5. The performance of multiscale opening preserves the shape of the liver and detects the first search region.

### 2.2.4. Second morphological filtering

In the clustering, instead of reducing the adjacent noise, any liver region can be reduced. To solve this problem, reverse filtering of the first morphological filtering is performed on the region of the original image corresponding to the previous labeled region. Therefore, multiscale morphological closing fills in holes and inlets that are smaller or narrower than the SE $B$. This processing recovers some regions of the liver that are damaged or reduced in the previous morphological filtering. The second search region is constructed based on the

result of the morphological closing, region-labeling, and modified K-means clustering similar to the previous processing. Multiscale morphological closing is defined, respectively, as

$$(f \bullet iB_n)(x, y) = ((f \oplus iB_n) \ominus (i + j)B_n)(x, y). \tag{6}$$

Final search range is determined by excluding the second search region from the first search region, as shown in Fig. 7. Since most of the liver boundaries are located in this search range, precise automatic liver segmentation is possible by using the deformable contour algorithm within this range. Furthermore, the initial liver boundary which will be a guidepost for search algorithm is constructed by extension of the second search region to original liver size. Fig. 8 shows the initial liver boundary.

## 2.3. Contour-based liver segmentation

The initial liver boundary acquired by multiscale morphological filtering is coarse liver contour. Therefore, we present the labeling-based search algorithm that deforms the initial liver boundary within the search range to find clear and final liver contour. For the search algorithm, we make gradient-label map.

### 2.3.1. Gradient-label map

Since the slice thickness of our CT data set is 5 mm, PVE is occurred at the boundary of adjacent object. Because occurrences of PVE yield a gradual intensity fall across the boundaries of objects, labeling-based search algorithm with an intensity partition that is sufficiently fine results in labeled images whose isolabel contours form conspicuous patterns. Because isolabel-contour patterns resemble isoelevation contours on topographical maps we refer to the labeled images as isolabel-contour maps. If we observe an area within an isolabel-contour map that extends from one object's center to its boundary within the search range, we see a distinct pattern. Where the intensity gradient is monotonic in raw image, the pattern of labels in the isolabel-contour map is monotonic as well. We observe dense contour patterns in the areas of abrupt intensity gradients and widespread contour patterns in the areas of gradual intensity gradients [4]. To make gradient-label map, we enhance the isolabel-contour map by using gradient magnitude into the weighing factor.

The spatial gradient of the search range image is approximated by use of a morphological gradient operator. The morphological gradient operator used is expressed such as

$$G(f) = \delta(f) - \varepsilon(f), \tag{7}$$
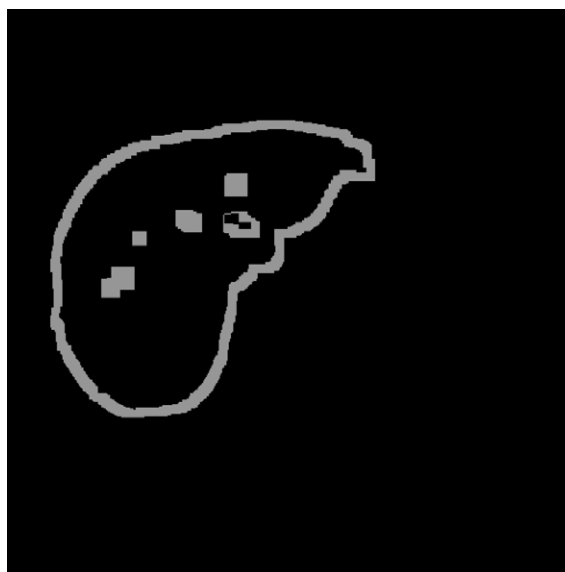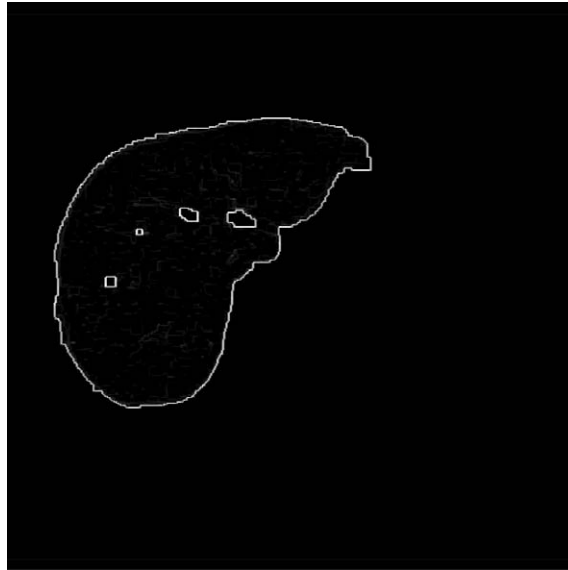


Fig. 7. Search range.

Fig. 8. Initial liver boundary.

where $\delta(f) = (f \oplus B_n)(x,y)$ and $\varepsilon(f) = (f \ominus B_n)(x,y)$. Note that the morphological gradient is positive. The positive gradients usually indicate borders between neighbor regions [8]. The gradient image is shown in Fig. 9 and exhibits large value along the region boundaries. The gradient image within the search range is reversed and normalized. Fig. 10 shows the gradient-label map.

### 2.3.2. Labeling-based search algorithm

PVEs may result in saddle-like patterns for tortuous structures whose plane of curvature is perpendicular to the image plane or for vessels that branch in the through-plane direction [4]. Fig. 11A shows examples of saddle-like patterns.
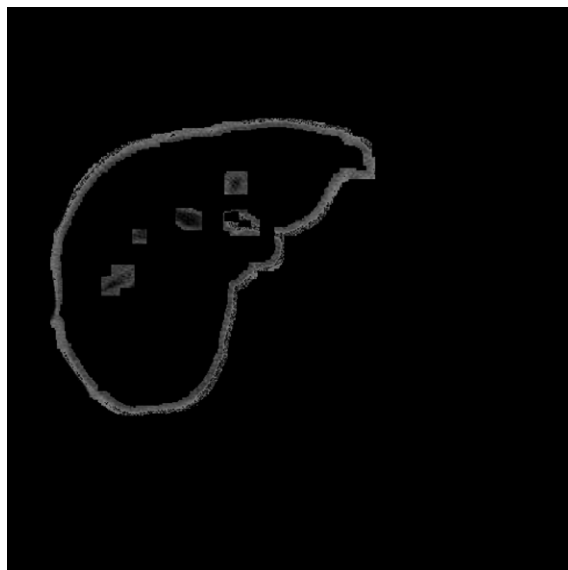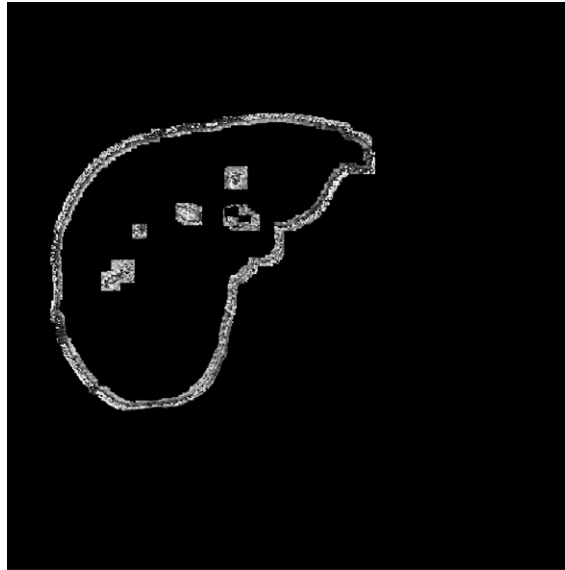


Fig. 9. Gradient image.

Fig. 10. Gradient-label map.

We can describe the entire pattern of liver contours as a relationship of the intensity distribution. This description allows us to manipulate pixels easily that are related to contours. Figs. 11B, C, and D show the pattern of contours and the intensity distribution of each pattern. We can classify the entire pattern into the three cases. In the first case, the liver is adjacent to the air region which has low intensity value. The second is the case that liver is touched to the ribs or the kidney which has high intensity value. In the last case in which the liver is adjoined to the stomach or the lung, the intensity value within the liver boundary is distributed through the low gray level.

The deformable contouring is started from the lowest located pixel of the initial liver contour toward the clockwise direction on gradient-label map. Fig. 12 shows the eight directions which the current pixel can proceed. Liver boundary is smooth since the liver is human organ. Therefore, the directions that the current pixel can proceed are three directions indicated by the small arrows in Fig. 12. Among the three directions, the center direction is determined by the initial liver contour obtained in the second stage. If the current pixel is located on the initial liver contour, then the next direction is determined by the initial liver contour. Otherwise, the next direction is same as the previous direction. The other two possible directions are on either side of the center direction, as shown in Fig. 12. All of three directions are the candidate pixels.

For the optimal path from each pixel, we formulate the local cost function at each candidate pixel. We can get a correct liver contour by finding optimal path which is the minimal cost value. The local cost function combining tree features is defined as

$$l(p,q) = w_D \cdot f_D(p,q) + w_B \cdot f_B(q) + w_I \cdot f_I(q), \qquad (8)$$

where each $w$ is the weight of the corresponding feature function. Experimentally, weights of $w_D = 0.3$, $w_B = 0.3$, and $w_I = 0.4$ seem to work well. The $p$ and $q$ are two neighboring pixels in the gradient-label map, and $l(p,q)$ represents the local cost on the directed link from $p$ to $q$ [11]. The $f_D$ is a function of gradient direction, and the two pixel value components, $f_B$ and $f_I$, are "initial boundary" and "intensity distribution" cost functions.

The gradient direction or orientation adds smooth constraint to the boundary by associating a relatively high cost for sharp changes in boundary direction. The gradient direction is simply the direction of the unit vector defined by $I_x$ and $I_y$. Therefore, by letting $D(P) = [I_x(p), I_y(p)]$ be a unit vector of the gradient direction at a point $p$ and defining $D'(p) = [I_y(p), -I_x(p)]$ as the unit vector perpendicular to $D(p)$, then the formulation for the gradient direction feature cost is
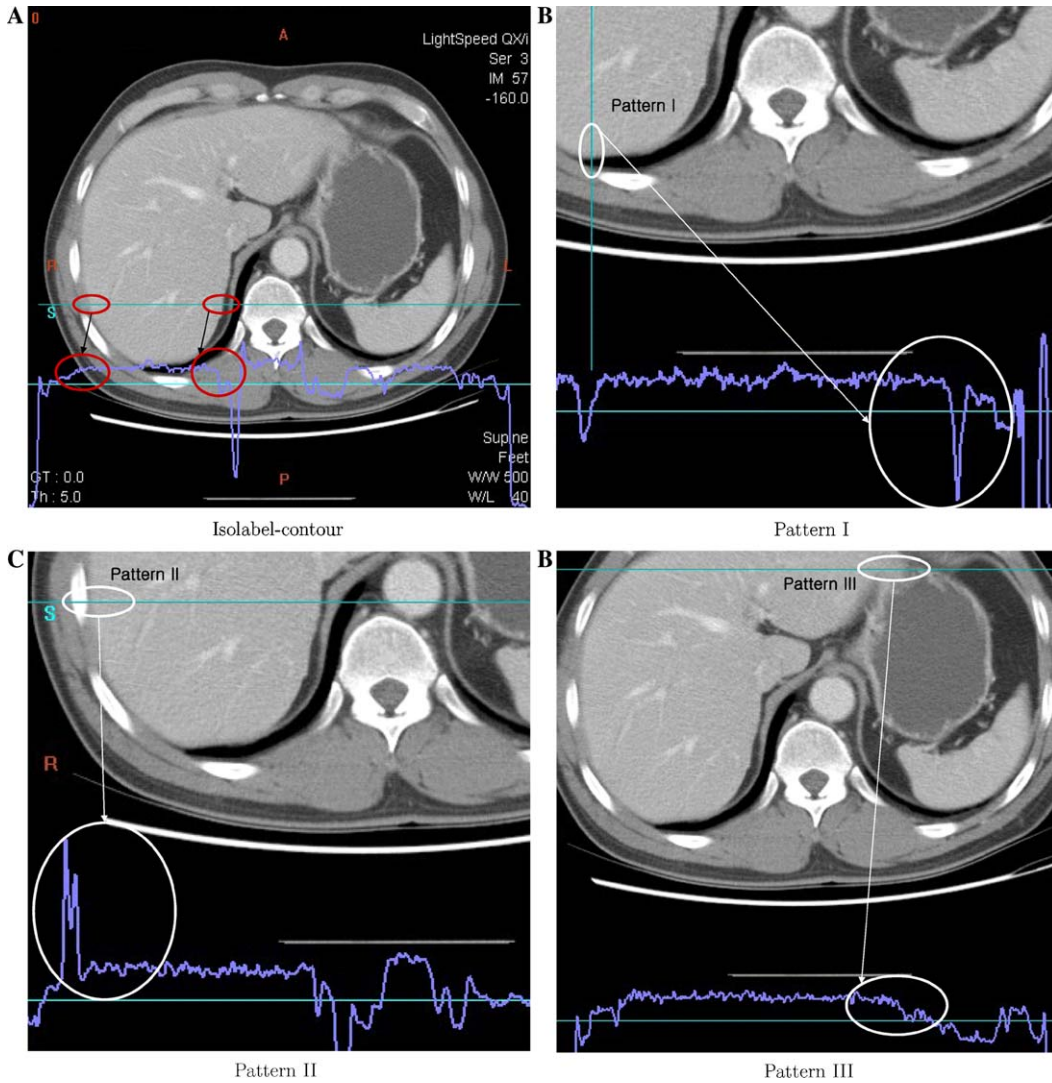
Fig. 11. Patterns of contour's intensity distribution: (B) adjacent to the air, (C) adjacent to the rib, (D) adjacent to the other organs.

$$f_D(p, q) = \frac{2}{3\pi} \{\text{acos}[d_p(p, q)] + \text{acos}[d_q(p, q)]\}, \tag{9}$$

where

$$
\begin{aligned}
d_p(p, q) &= D'(p) \cdot L(p, q) \\
d_q(p, q) &= L(p, q) \cdot D'(q)
\end{aligned}
\tag{10}
$$

are vector dot products and

$$L(p, q) = \frac{1}{\|p - q\|} \begin{cases} q - p; \text{ if } D'(p) \cdot (q - p) \geqslant 0 \\ p - q; \text{ if } D'(p) \cdot (q - p) < 0. \end{cases} \tag{11}$$

The $L(p,q)$ is normalized bidirectional link or unit edge vector between pixels $p$ and $q$ and simply computes the direction of the link between $p$ and $q$ so that the difference between $p$ and the direction of the link is minimized. Links are either horizontal, vertical, or diagonal (relative to the position of $q$ in $p$'s neighborhood) and point such that the dot product of $D'(p)$ and $L(p,q)$ is positive (i.e., the angle between $D'(p)$ and the link $\geqslant \frac{\pi}{2}$), as noted in Eq. 11 above. Therefore, the direction feature cost is low when the gradient direction of the two neighboring pixels are similar to each other and the link between them [11].
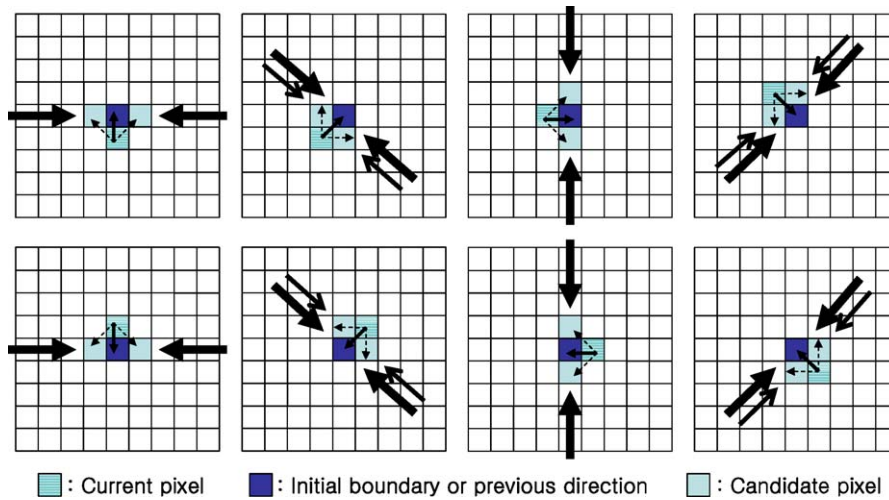
Fig. 12. Search pattern.

One of the two pixel components, $f_B(q)$ is the function estimating the state of the candidate pixel about the initial boundary. The state is inside or outside position in the gradient-label map. Function $f_B(q)$ is

$$f_B(q) = \frac{1}{255}\{I(q) \cdot s\}, \tag{12}$$

where $I(q)$ is the pixel value at $q$ and $s$ is the weight of the state. If pixel is "inside" and "outside," $s$ is 0.4. Otherwise $s$ is 0.2.

For the pixel component of the intensity distribution, we formulate cost function, $f_I(q)$, by following the search pattern, as shown in Fig. 12. Thus, the formulation for the intensity distribution pixel value, $f_I(q)$, for a given pixel $q$ is

$$f_I(q) = \frac{1}{255}\{I(q) \cdot P(n)\}, \tag{13}$$

where $P(n)$ indicates a kind of the pattern as mentioned above. Each pattern is decided by searching neighboring pixels of each candidate pixel on bidirectional large arrows within the $9 \times 9$ window, as shown in Fig. 12. If the current pixel goes to perpendicular direction, then the neighboring eight pixels of the candidate pixel that correspond to the initial boundary or previous direction are examined whether those are on the above pattern. The neighboring pixels within $9 \times 9$ window of the other candidate pixels are also examined. $P(n)$ value is experimentally determined but if the candidate pixel satisfies the pattern, $P(n)$ is generally from 0.2 to 0.4. Otherwise $P(n)$ is 1.

Deformable contouring is performed by computing the local cost function on gradient-label map. The result of the proposed algorithm is determined by deformable contouring of the initial liver boundary, as shown in Fig. 13.

## 3. Volume measurement based on the segmentation

For volume measurement of the liver, we calculate the volume by using thickness and interval information of the slice and size of the pixel. The following equation is for volume measurement using the previous segmented liver region [12].

$$\text{Volume} = \sum_{i=1}^{N-1}(((L_p * X * Y) \text{ of } S_i + (L_p * X * Y) \text{ of } S_{i+1})/2) * D, \tag{14}$$
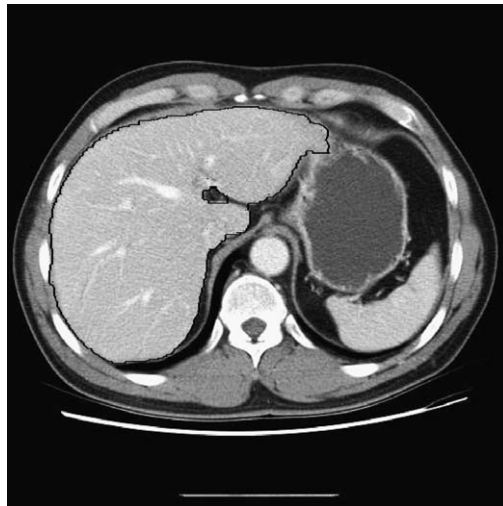
Fig. 13. Segmentation result.

where $N$ is the number of the slice including the segmented liver region, $S_i$ is the slice number, $D$ is the interval of the slice, $L_p$ is the number of the pixel in the segmented liver region, and $X, Y$ are the size of a pixel.

## 4. Experimental results and discussion

We experimented several samples with various shapes and irregular texture of 10 patients. All of the used samples are contrast-enhanced abdominal CT images of venous phase with 5 mm interval.
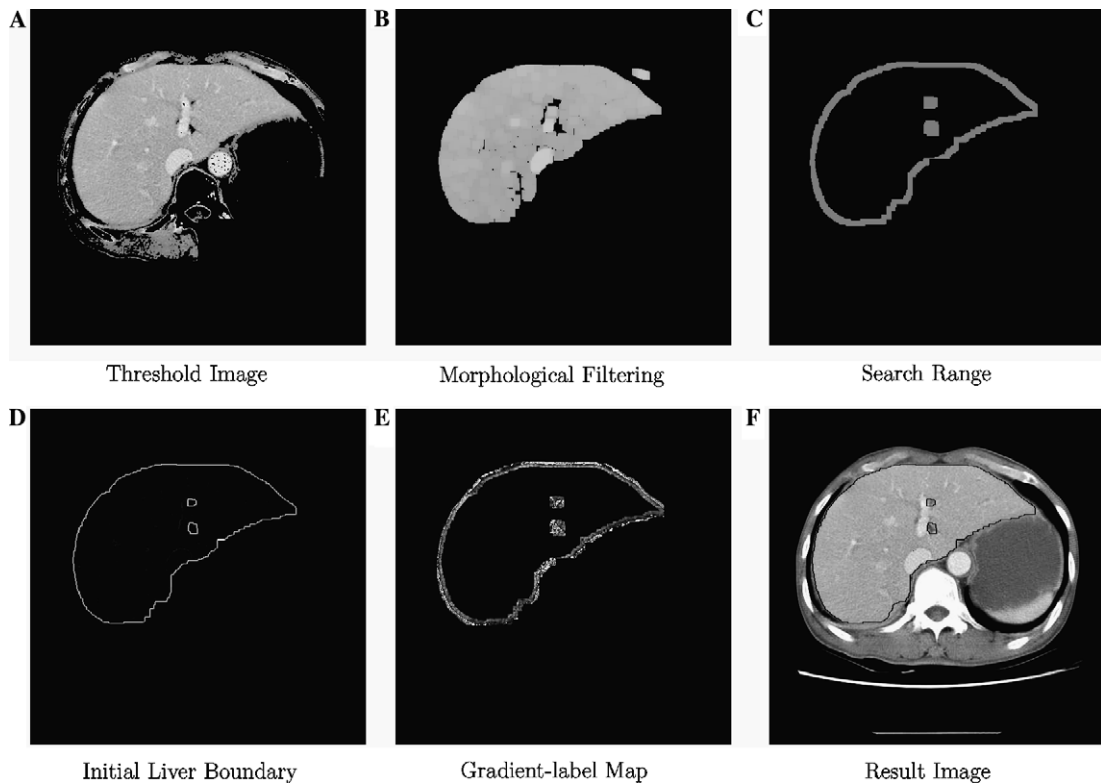


Fig. 14. Experiment of the patient 1.

Each sample shows the result of each process of the proposed algorithm, six images in total, such as threshold image, the result of morphological filtering, search range, initial liver boundary, gradient-label map, and the final result through Fig. 14 to Fig. 15.

Figs. 14A and 15B depict the multilevel threshold image on ROI blocks in the image simplification. Threshold value is determined by analyzing the intensity distribution of several samples that are the manually segmented liver and adjacent muscle. We can see that many other organs and tissues are reduced in the threshold image. However, unconnected or small tissues are remained. To reduce these objects and preserve the liver region, we performed the multiscale morphological filtering, as shown in Figs. 14B and 15B.

In the multiscale filtering, parameter $k$, an integer, representing the scale factor of SE $B$ and $n$ that is the size of $B$ is determined by analyzing of the result of thresholding. That is, parameter $k$ and $n$ are determined by checking the number of pixels that are remained on the ROI blocks and considered pixels of air region after multilevel thresholding. This process is for more precise preservation of the liver region. The initial liver region is obtained by performing region-labeling and clustering. For searching the correct liver contour, we make the search range by recursive morphological filtering. The appropriate composition of the order of morphological operations makes the suitable search range for liver contour as depicted in Figs. 14C and 15C. In addition, for deformable contouring, we construct the initial liver boundary, as shown in Figs. 14D and 15D.

Lastly, deformable contouring based on labeling-based search algorithm delineates the final liver contour in search range. Figs. 14E and 15E indicate the gradient-label map weighted by gradient image. Final result is determined by the compute of local cost function, as shown in Figs. 14F, 15F, and 16.

The results of the proposed algorithm were evaluated by comparing with the results of manual tracing as a gold standard by experts. The comparable measure used is exclusive-or method. This method can detect the fault positive and negative error. The average correctness of the segmentation is about 96%. It shows the proposed algorithm is effective automatic segmentation scheme of the liver in CT images.

Volume measurement is performed by using the above segmentation results. Tables 1 and 2 show the comparison of automatic and manual segmentation for volume measurement of two different livers.
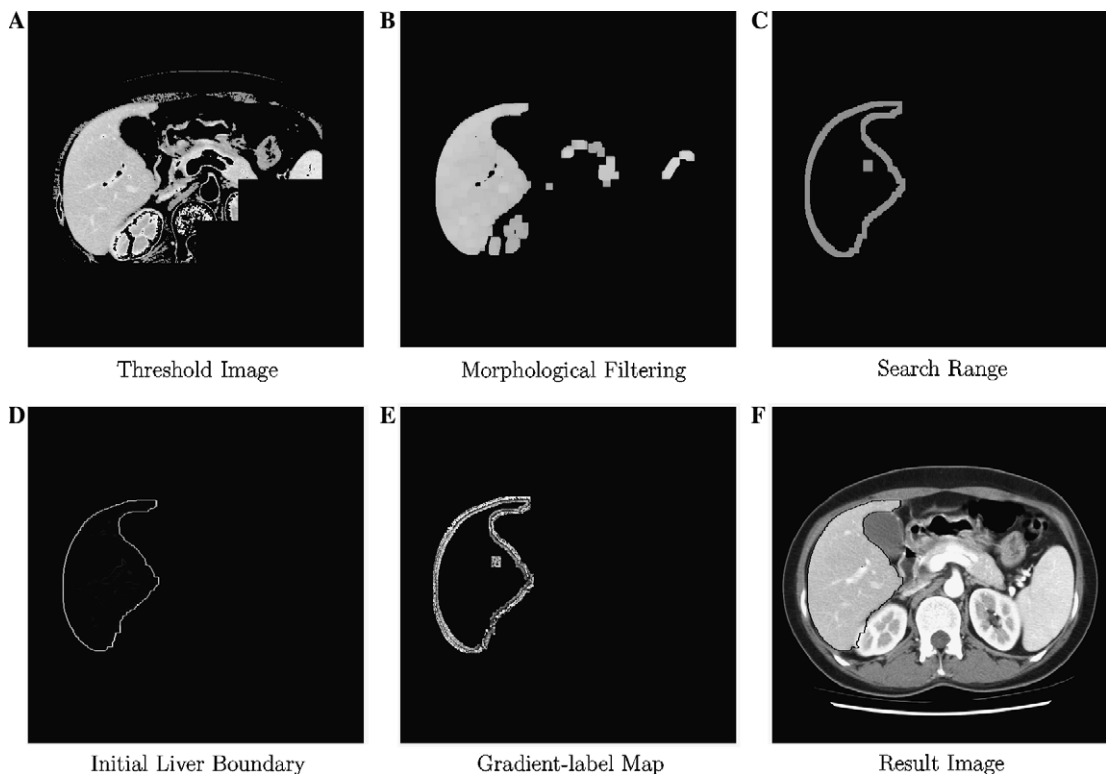


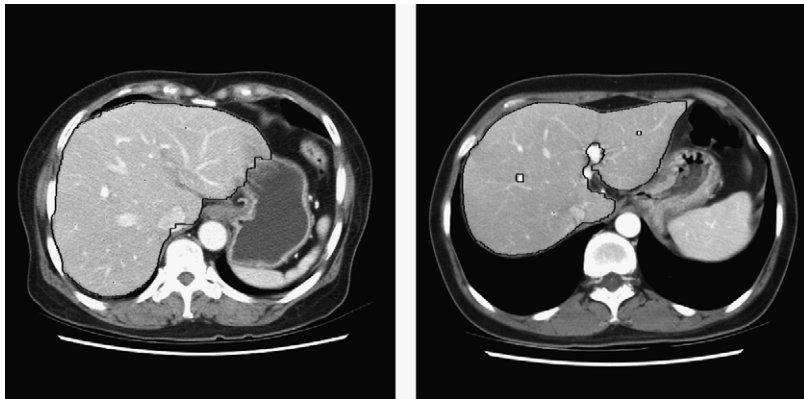Fig. 15. Experiment of the patient 2.

Fig. 16. Experimental result of the patient 3 and patient 4.

Table 1
Comparison 1 of automatic vs. manual segmentation of the liver (mm$^2$)

| Sample number | Automatic | Manual | Error rate (%) |
| --- | --- | --- | --- |
| 1 | 4570.03 | 4600.03 | 0.652 |
| 2 | 9432.12 | 9322.13 | −1.180 |
| 3 | 14359.81 | 14254.97 | −0.735 |
| 4 | 12672.21 | 12576.27 | −0.763 |
| 5 | 12541.24 | 12688.73 | 1.162 |
| 6 | 13121.12 | 13017.53 | −0.796 |
| 7 | 11494.59 | 11584.49 | 0.776 |
| 8 | 9420.27 | 9555.81 | 1.418 |
| 9 | 7611.03 | 7845.35 | 2.987 |
| 10 | 6125.13 | 6061.23 | −1.054 |
| 11 | 5310.97 | 5274.00 | −0.701 |
| 12 | 4621.27 | 4699.13 | 1.657 |
| 13 | 4006.03 | 4033.93 | 0.692 |
| 14 | 3524.13 | 3605.53 | 2.258 |
| 15 | 3007.97 | 3026.56 | 0.614 |

Table 2
Comparison 2 of automatic vs. manual segmentation of the liver (mm$^2$)

| Sample number | Automatic | Manual | Error rate (%) |
| --- | --- | --- | --- |
| 1 | 3470.03 | 3531.83 | 1.750 |
| 2 | 3910.11 | 4002.98 | 2.320 |
| 3 | 5490.59 | 5543.22 | 0.950 |
| 4 | 9141.62 | 8942.69 | −2.240 |
| 5 | 12817.14 | 12394.59 | −3.409 |
| 6 | 13762.82 | 13836.11 | −0.530 |
| 7 | 13611.91 | 13699.13 | 0.637 |
| 8 | 13291.01 | 13119.94 | −1.304 |
| 9 | 12877.20 | 12991.73 | 0.882 |
| 10 | 9951.23 | 10314.36 | 3.521 |
| 11 | 7812.37 | 7897.15 | 1.074 |
| 12 | 6395.71 | 6169.17 | −3.672 |
| 13 | 5519.07 | 5341.12 | −3.332 |
| 14 | 4710.87 | 4891.89 | 3.703 |
| 15 | 4132.70 | 4197.11 | 1.535 |
| 16 | 3727.95 | 3781.98 | 1.429 |
| 17 | 3499.25 | 3544.57 | 1.279 |
| 18 | 3073.89 | 3101.93 | 0.904 |
| 19 | 2618.92 | 2631.32 | 0.471 |

Table 3
Comparison of automatic vs. manual segmentation in volume measurement of the liver (L)

| Case | Automatic | Manual | Error (%) |
|------|-----------|--------|-----------|
| CT 1 | 1.321427 | 1.321821 | 0.030 |
| CT 2 | 1.101013 | 1.099298 | −0.156 |
| CT 3 | 1.135722 | 1.141217 | 0.482 |
| CT 4 | 1.551525 | 1.608771 | 3.558 |
| CT 5 | 1.276392 | 1.239157 | −3.010 |
| CT 6 | 1.399148 | 1.434772 | 2.483 |

Table 3 presents the comparison of automatic and manual segmentation in volume measurement of the liver. The average error rate of volume measurement is 3%. Even though the proposed algorithm involves so many preprocessing steps, computational complexity is not bad. The processing time of image simplification and search range detection takes about 20–60 s/slice and contour-based segmentation takes some more time because it is similar to dynamic programming being less than $O(n)$ for a contour having $n$ points which are allowed to move to next point (Fig. 12). Total processing time is normally about 1–3 min/slice on Pentium 4 3.0 GHz system.

## 5. Conclusions

In this paper, we have proposed an automatic segmentation algorithm for volume measurement of the liver using a priori knowledge and the deformable contour method based on morphological filtering. The proposed algorithm using multilevel thresholding based on the analysis of the intensity distribution within ROI decrease the needless computation time and efforts by reducing the regions of the other organs and tissues. In addition, multiscale morphological filtering using region-labeling and clustering detects the initial liver boundary and the search range for the deformable contouring. The final contour is found by using the labeling-based search algorithm on the gradient-label map. Search algorithm considering partial-volume effect (PVE) computes the minimum cost function composed of the gradient magnitude, the gradient direction, and the pattern of the intensity distribution. The final results are compared to manually segmented image and manually volume measured results by the radiologist, and we could know that the fault positive/negative error is almost not existed. This algorithm is the effective automatic segmentation algorithm of the liver in CT images for the first step of the computer-aided diagnosis (CAD) and computer-aided surgery (CAS) systems.

## Acknowledgments

## References

[1] E.L. Chen, P.C. Chung, C.L. Chen, H.M. Tsai, C.I. Chang, An automatic diagnosis system for CT liver image classification, IEEE Trans. Biomed. Eng. 45 (6) (1998) 783–794.
[2] S.J. Lim, Y.Y. Jeong, C.W. Lee, Y.S. Ho, Automatic segmentation of the liver in CT images using the watershed algorithm based on morphological filtering, SPIE Proc. 5370 (2004) 1658–1666.
[3] M.L. Giger, N. Karssemeijer, S.G. Armato III, Guest editorial: computer-aided diagnosis in medical imaging, IEEE Trans. Med. Imaging 20 (12) (2001) 1205–1208.
[4] S. Shiffman, G.D. Rubin, S. Napel, Medical image segmentation using analysis of isolable-contour maps, IEEE Trans. Med. Imaging 19 (11) (2000) 1064–1074.
[5] S. Mukhopadhyay, B. Chanda, Multiscale morphological segmentation of gray-scale images, IEEE Trans. Image Process. 12 (5) (2003) 533–549.
[6] B. Reitinger, A. Bornik, R. Beichel, Efficient volume measurement using voxelization, in: Proceedings of Spring Conference on Computer Graphics 2003, 2003.

[7] R.C. Gonzalez, R.E. Woods, Digital Image Processing, Prentice-Hall, Englewood Cliffs, NJ, 2002.

[8] M.C. Kim, J.G. Choi, D.H. Kim, H. Lee, M.H. Lee, C.T. Ahn, Y.S. Ho, A VOP generation tool: automatic segmentation of moving objects in image sequences based on spatio-temporal information, IEEE Trans. Circuits Syst. Video Technol. 9 (8) (1999) 1216–1226.

[9] P. Maragos, Pattern spectrum and multiscale shape representation, IEEE Trans. Pattern Anal. Mach. Intell. 11 (1989) 701–716.

[10] E. Gose, R. Johnsonbaugh, S. Jost, Pattern Recognition and Image Analysis, Prentice-Hall, Englewood Cliffs, NJ, 1996.

[11] E.N. Mortensen, W.A. Barrett, Interactive segmentation with intelligent scissors, Graph. Model Im. Proc. 60 (1998).

[12] H.Y. Kim, Computer Based Automatic Segmentation and Volume Measurement of the Liver and Spleen in Contrast-Enhanced Helical CT Images, A Thesis for the degree of Doctor of Philosophy of Medicine in Chungnam National University, 2002.